Excitation energy dependence of 3d-metal $L_{2,3}$ x-ray emission spectra of $M[N(CN)_2]_2$ (M = Mn, Fe, Co, Ni, Cu) near 2p threshold

2005 J. Phys.: Condens. Matter 17 7307

(http://iopscience.iop.org/0953-8984/17/46/014)

INSTITUTE OF PHYSICS PUBLISHING JOURNAL OF PHYSICS: CONDENSED MATTER

J. Phys.: Condens. Matter **17** (2005) 7307–7318 doi:10.1088/0953-8984/17/46/014

Excitation energy dependence of 3d-metal $L_{2,3}$ x-ray emission spectra of $M[N(CN)_2]_2$ (M = Mn, Fe, Co, Ni, Cu) near 2p threshold

S Kučas[1], A Kynienė[1], R Karazija[1], L D Finkelstein[2] and E Z Kurmaev[2]

[1] Vilnius University, Institute of Theoretical Physics and Astronomy, A Goštauto 12, Vilnius LT 01108, Lithuania
[2] Institute of Metal Physics, Russian Academy of Sciences—Ural Division, 620219 Yekaterinburg GSP-170, Russia

Received 1 June 2005, in final form 15 September 2005
Published 1 November 2005
Online at stacks.iop.org/JPhysCM/17/7307

Abstract

Measurements of resonant inelastic x-ray spectra (RIXS) of $M[N(CN)_2]_2$ (M = Mn, Fe, Co, Ni, Cu) molecular magnets are performed near 2p-threshold excitation. The $L_{2,3}$ x-ray emission spectra reveal features in fine structure in dependence on excitation energy, some of which are common for all 3d elements and others are typical only for the elements located in the middle (Mn, Fe, Co) or at the end of the series (Ni, Cu). The relative role of two channels for radiative decay from the excited (RXES, resonant x-ray emission spectra) and the ionized (NXES, non-resonant x-ray emission spectra) states under variation of atomic number of 3d element is discussed. The full atomic calculation of RIXS spectra for a whole energy range of excitation energies is presented for $Mn[N(CN)_2]_2$. A reasonable agreement is found for the shape, the relative intensities and dynamics of energy position for the experimental and calculated RXES. This evidences of many-electron nature of resonance x-ray emission spectra, at least for Mn. In contrast, we could not describe the non-resonant x-ray emission spectra in the atomic approach because the Coster–Kronig transitions $2p_{1/2}^{-1}3d^N \rightarrow 2p_{3/2}^{-1}3d^{N-1} + e$ were forbidden energetically in free ions though allowed in solids.

1. Introduction

Since the discovery of the magnetic ordering in molecular magnets at room temperature, these systems have attracted great attention over the past decade [1, 2]. Molecular magnets consist of magnetic metal ions that are coordinated with non-magnetic organic species. The metal ions provide magnetic moments while the organic species provide superexchange pathways between the magnetic centres. It has been established that compounds containing transition-metal ions with six or fewer electrons in the 3d orbitals will order as canted antiferromagnets while the

ones with seven or more electrons do arrange ferromagnetically [3, 4]. Previous studies of the series of isostructural $M[N(CN)_2]_2$ (M = Mn, Fe, Co, Ni, Cu) have found $Mn[N(CN)_2]_2$ and $Fe[N(CN)_2]_2$ to be antiferromagnets, $Co[N(CN)_2]_2$ and $Ni[N(CN)_2]_2$ to be ferromagnets and $Cu[N(CN)_2]_2$ to be a paramagnet [5, 6]. In this respect this series is ideally suited to study how the successive population of the 3d shell induces different magnetic ordering in molecule-based magnetic systems. In our previous work [7] we gave a detailed theoretical and experimental study of the electronic structure of the entire $M[N(CN)_2]_2$ (M = Mn, Fe, Co, Ni, Cu) series by comparing *non-resonant* x-ray emission spectra of the transition metals with x-ray photoelectron spectra and our electronic structure calculations. It is found that the binding energy of the M 3d bands and the hybridization between N 2p and M 3d states both increase in going across the row from M = Mn to Cu. Calculations indicate that the ground-state magnetic ordering, which varies across the series, is mainly dependent on the occupation of the metal 3d shell and that structural differences in the superexchange pathways for different compounds play a secondary role. For M = Mn, Co and Ni calculated ground states correspond to experimental ones [5, 6]. For M = Fe and Cu the possible discrepancies are discussed.

The present paper pays the main attention to discussion of the resonant phenomena of $M[N(CN)_2]_2$ compounds and gives a detailed theoretical analysis of the excitation energy dependence of $L_{2,3}$ resonant x-ray emission spectra (RXES) based on atomic calculations for $Mn[N(CN)_2]_2$.

2. Experimental details

The soft x-ray emission measurements were performed at Beamline 8.0.1 of the Advanced Light Source at Lawrence Berkeley National Laboratory. Transition metal $L_{2,3}$ ($3d, 4s \rightarrow 2p$ transitions) RXES were measured, employing the soft x-ray fluorescence endstation. To minimize the radiation damage of the samples during x-ray fluorescent measurements the sample holder was shifted laterally before each measurement to expose a fresh part of the sample to the beam.

The energy resolution of the 3d metal $L_{2,3}$ XES is 0.7–0.8 eV. $L_{2,3}$ x-ray absorption spectra were measured in total electron yield mode (TEY) monitoring the sample current. For $Co[N(CN)_2]_2$, $Ni[N(CN)_2]_2$ and $Cu[N(CN)_2]_2$ compounds the excitation energies for measurements of resonant inelastic x-ray spectra (RIXS) are selected using $L_{2,3}$ TEY measurements of pure metals. Polycrystalline pressed pellets of each $M[N(CN)_2]_2$ compound were used for the measurements. Details of the preparation of samples are given in [5, 6].

3. Results and discussion

3.1. Experimental spectra

Resonantly excited $L_{2,3}$ XES of 3d elements opened a new page in x-ray emission spectroscopy. The studies of excitation energy (E_{exc}) dependence of $L_{2,3}$ XES have revealed that variation of the fine structure of XES with E_{exc} is due to the influence of intra-atomic multiplet effects, arising from Coulomb direct and exchange interactions between the 2p hole and 3d electrons in the intermediate state of common absorption–emission process and also due to the solid state effects which modify an atomic picture [8]. Unlike the intra-atomic interactions, which can be calculated with high accuracy, an influence of solid-state effects can be taken into account roughly using cluster methods with adjustable parameters [9].

It is found that not only the shape and energy position of resonant spectra is changed with E_{exc} but also a sharp increase of $I(L_2)/I(L_3)$ intensity ratio takes place when the excitation

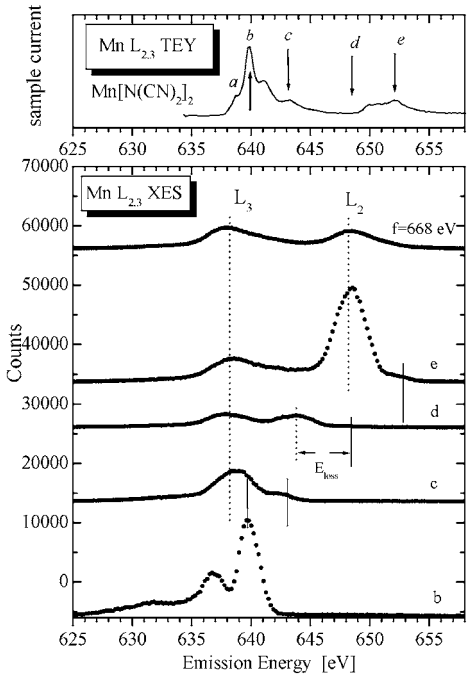

Figure 1. Mn $L_{2,3}$ XAS (top) and Mn $L_{2,3}$ RXES (bottom) of $Mn[N(CN)_2]_2$.

energy passes the $2p_{1/2}$ threshold. All $L_{2,3}$ XES features show distinct dependence on the atomic number of the d element and in the present paper we will discuss all these problems. Among 3d elements, Mn occupies a special place because of the exchange-stabilized ^6S ground state, which essentially decreases the relative role of solid state effects as well as strongly limiting the possible excitations. For this reason an atomic calculation reproduced RIXS for MnO for the whole energy range of Mn 2p XAS [10]. However, that paper does not consist of the intensity calculation of resonantly excited $L_{2,3}$ XES and in this respect the present paper fills this gap. $Mn[N(CN)_2]_2$ is a very suitable object for the comparison of the experiment with the atomic calculation because Mn–Mn interaction in this compound is very weak and we can neglect it.

RIXS spectra of 3d elements for $M[N(CN)_2]_2$ (M = Mn, Fe, Co, Ni, Cu) are presented in figures 1–3. As seen, a general feature of the resonant excitation is connected with the sharp increase of the $I(L_2)/I(L_3)$ intensity ratio when E_{exc} coincides with the L_2 threshold compared with the excitation above the L_2 threshold[3]. This effect is due to the preferential excitation from the L_2 subshell at E_{exc} on the L_2 threshold. The diminished dependence of the $I(L_2)/I(L_3)$ intensity ratio with atomic number of the d element is shown in figure 4. This dependence is revealed at any E_{exc} and as shown in [11] is due to the smooth increase of $f_{2,3}$ Coster–Kronig (C–K) parameter from 0.39 for Mn to 0.47 for Cu [12].

We have also observed the essential differences between RIXS spectra for different d elements whose value depends on their atomic number, besides the common (for all of them) effect of the increase of $I(L_2)/I(L_3)$ intensity ratio at L_2 threshold. They arise from the ratio between two radiation channels: NXES (non-resonant x-ray emission) and RXES (resonant x-ray emission). The first channel is realized in the preliminary ionized atoms by

[3] This effect is also observed in $L_{2,3}$ RXES of 3d metals and analysed by us in [11].

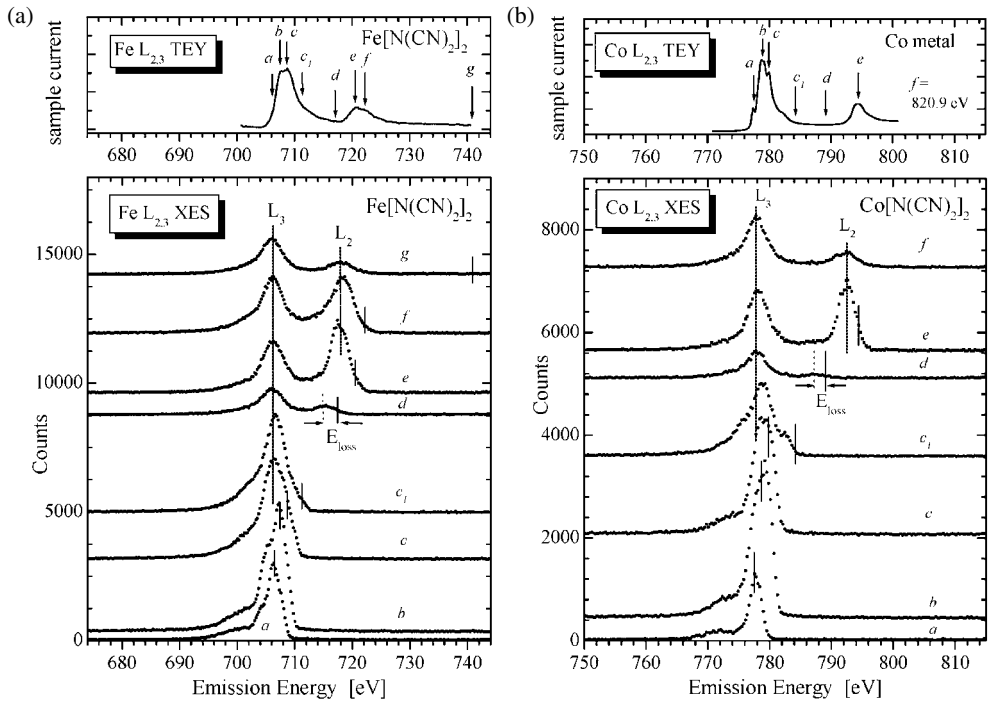

Figure 2. (a) Fe $L_{2,3}$ XAS (top) and Fe $L_{2,3}$ RXES (bottom) of $Fe[N(CN)_2]_2$. (b) Co 2p $L_{2,3}$ (top) and Co $L_{2,3}$ RXES (bottom) of $Co[N(CN)_2]_2$.

passing from the initial p^6d^N to the intermediate $p^{-1}d^N$ + e (outside atom) and the second one in preliminary excited atoms by passing within act of absorption from initial p^6d^N to intermediate $p^{-1}d^{N+1}$. An independence of the energy of main maxima of $L_{2,3}$ spectra from E_{exc} is characteristic of NXES because radiation takes place from the occupied valence states, whereas the high energy shift of energy peaks is observed in RXES with E_{exc}. In this case the redistribution of RXES intensity from the elastic peak at E_{exc} near the L_3 threshold to inelastic peaks located at the lower emission energies for E_{loss} takes place when E_{exc} is shifted between L_3 and L_2 thresholds. The elastic lines at the L_2 threshold are pronounced very weakly.

As seen from figures 1 to 3, for Mn, Fe and Co the NXES arise only when E_{exc} passes out of the main maximum of L_3 XAS and is going to its slope. Up to this moment the emission decay is most probable via the RXES channel. For Ni and Cu spectra the situation is different and NXES appears at once when E_{exc} reaches the L_3 threshold, and RXES does not appear at all. We suppose that such a decrease of RXES intensity (in respect to NXES) with number of electrons in the 3d shell corresponds to the decreasing of the excitation cross-section in respect to the ionization cross-section, as has been observed in XES of the rare-earth elements for the 4f → 4d [13] and 5p → 4d [14] transitions.

3.2. Atomic calculations

3.2.1. Theoretical model and its application to x-ray absorption and energy level spectra. The model of the free atom has been applied for the calculation of $L_{2,3}$ x-ray emission spectra of Mn in the compound $Mn[N(CN_2)]_2$. We have used the pseudorelativistic Hartree–Fock

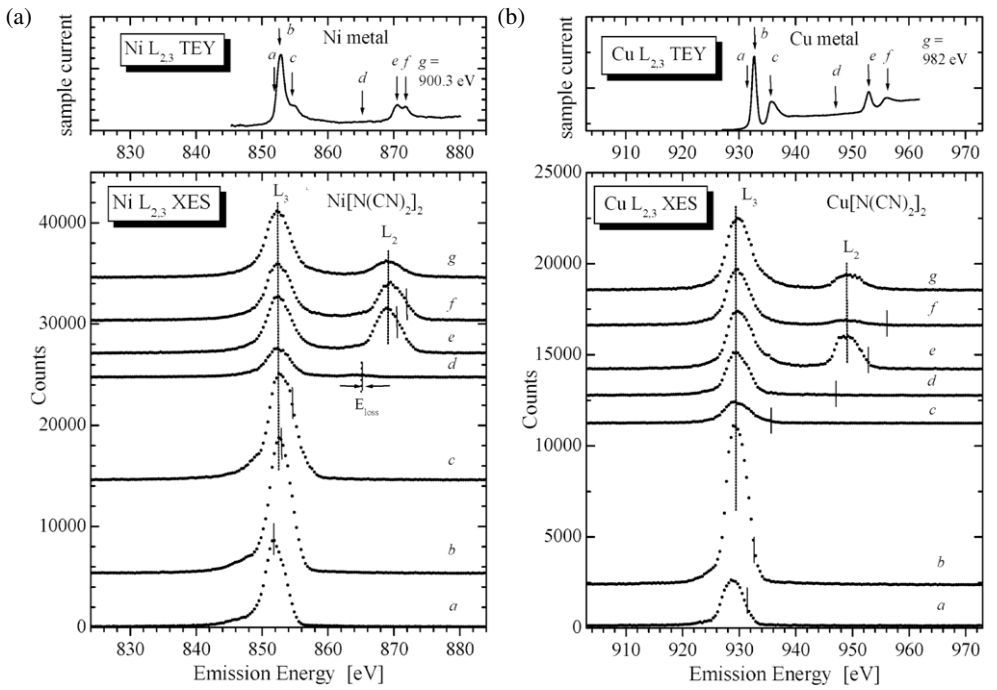

Figure 3. (a) Ni $L_{2,3}$ XAS (top) and Ni $L_{2,3}$ RXES (bottom) of $Ni[N(CN)_2]_2$. (b) Cu $L_{2,3}$ XAS (top) and Cu $L_{2,3}$ RXES (bottom) of $Cu[N(CN)_2]_2$.

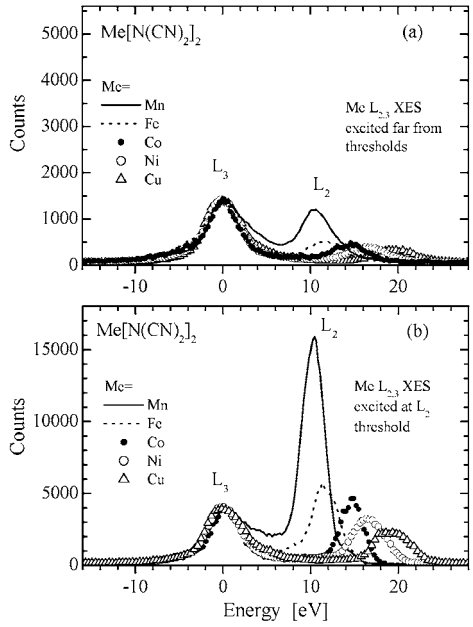

Figure 4. NXES (top) and RXES (bottom) spectra of $M[N(CN)_2]_2$ (M = Mn, Fe, Co, Ni, Cu).

Table 1. The natural widths of levels mostly populated by photoabsorption of the $2p^{-1}3d^64s^2$ configuration.

J of $2p^5$	Term of $3d^6$	J	E with respect to the ground level of $2p^63d^54s^2$ (eV)	Width (eV)	Deviation from the average width (%)
1.5	$^5D_{2.0}$	3.5	641.667	0.30	26.67
1.5	$^5D_{1.0}$	2.5	641.879	0.30	25.54
1.5	$^5D_{0.0}$	1.5	642.060	0.32	19.82
1.5	$^5D_{4.0}$	2.5	642.208	0.37	2.66
1.5	$^5D_{2.0}$	1.5	642.338	0.42	8.02
1.5	$^5D_{3.0}$	3.5	642.406	0.32	17.80
1.5	$^5D_{2.0}$	2.5	642.623	0.32	18.02
1.5	$^5D_{4.0}$	3.5	643.329	0.32	17.28
1.5	$^5D_{3.0}$	2.5	643.533	0.32	19.54
1.5	$^5D_{2.0}$	1.5	643.727	0.31	21.82
1.5	$^3P_{2.0}$	3.5	643.790	0.33	14.20
1.5	$^3P_{1.0}$	2.5	644.107	0.33	17.45
1.5	$^3G_{3.0}$	3.5	645.308	0.36	6.49
1.5	$^3P_{2.0}$	2.5	645.651	0.36	6.01
1.5	$^3D_{2.0}$	3.5	645.720	0.37	1.93
1.5	$^3D_{3.0}$	3.5	646.354	0.37	4.49
0.5	$^5D_{2.0}$	1.5	652.397	0.33	15.40
0.5	$^5D_{3.0}$	2.5	652.454	0.34	12.62
0.5	$^5D_{4.0}$	3.5	652.715	0.35	8.66
0.5	$^5D_{1.0}$	1.5	653.497	0.36	6.85
0.5	$^5D_{2.0}$	2.5	653.932	0.39	3.12
0.5	$^5D_{3.0}$	3.5	654.173	0.40	4.79
Average Auger width				0.38	

method [15]; the calculations have been performed with the Cowan code. The theoretical values of the Coulomb integrals F^k and G^k have been diminished by a scaling factor of 0.75 to account for some effects of correlations between electrons.

The calculated spectra have been convoluted taking into account the Lorentzian natural profile and the Gaussian instrumental profile. The instrumental width for the photoabsorption spectrum has been taken equal to 0.4 eV, and for the x-ray emission spectra equal to 0.65 eV.

For Mn the fluorescence yields $\omega(L_2)$ and $\omega(L_3)$ have rather small values, which do not exceed 0.005, thus we can neglect the contribution of radiative transitions to the natural widths of levels and take into account only the Auger widths.

The natural width of level for the configuration containing not only an inner vacancy but also an open shell depends on many-electron quantum numbers. This dependence for some levels mostly populated by photoabsorption is shown in table 1. The difference from the average width can reach for some levels 25% and more. When many lines with different widths cover themselves, taking into account the term-dependence of width practically does not lead to the change of absorption spectrum. However, more significant changes of some maxima, corresponding to the energetically separate lines, are possible in the emission spectra. Thus the more accurate values of widths have been used in all calculations.

The initial process populating levels of excited and ionized atoms is photoabsorption. Thus at first the validity of the model has been investigated for the x-ray absorption or corresponding to it the total electron yield spectrum.

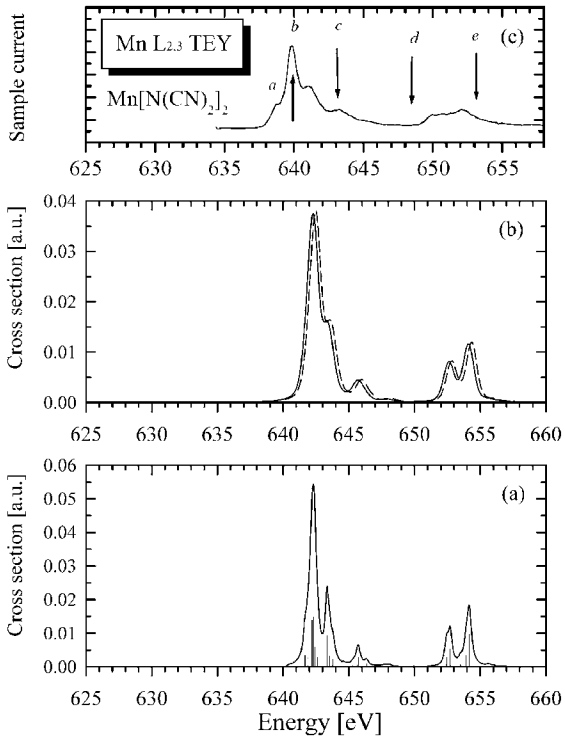

Figure 5. 2p photoabsorption spectrum of Mn: (a) photoexcitation spectrum of free atom (only the natural widths of lines are taken into account); (b) photoexcitation spectrum of Mn (——) and Mn^{2+} (- - - -) (the natural widths of lines and the instrumental width are accounted for); (c) experimental total electron yield spectrum of Mn in $Mn[N(CN_2)]_2$.

Initially an Mn atom with a half filled $3d^5$ shell is in the ground $^6S_{2.5}$ state. The main structure of the photoabsorption spectrum is determined by photoexcitation to various levels of the $2p^{-1}3d^6$ configuration. The transitions from the level with the orbital moment equal to zero and maximal multiplicity are constricted by the selection rules for the electric dipole transitions: all main lines correspond to transitions to the levels of the single ^5D term of the d^6 shell. The low energy group of lines at 641–648 eV is produced by the excitations from the $2p_{3/2}$ subshell and the high energy group at 652–657 eV by the excitations from the $2p_{1/2}$ subshell (figure 5(a)). These two groups are energetically separated due to the almost forbidden excitations to the levels of other terms (in this interval only very weak lines exist). For the same reason the excitation lines practically disappear above 657 eV, though the interval of possible excitation for the free Mn atom extends up to 663 eV.

The calculated photoabsorption spectra for Mn and Mn^{2+} (without the $4s^2$ electrons) are rather similar and their main structure corresponds to the experimental spectrum of Mn in the investigated compound (figure 5(b)). The shift of energy positions by about 2–2.5 eV in free atoms or ions with respect to the compound remains due to the solid state and probably correlation effects. The presence of $4s^2$ electrons also brings a slight influence on the photoexcitation as well as on the Auger and radiative transition rates. These electrons have a larger influence on the relative positions of energy levels of different configurations. As seen from figure 1 the low-energy maximum *a* is not reproduced in the calculated spectrum probably because it is connected with a splitting of low terms by a crystal field.

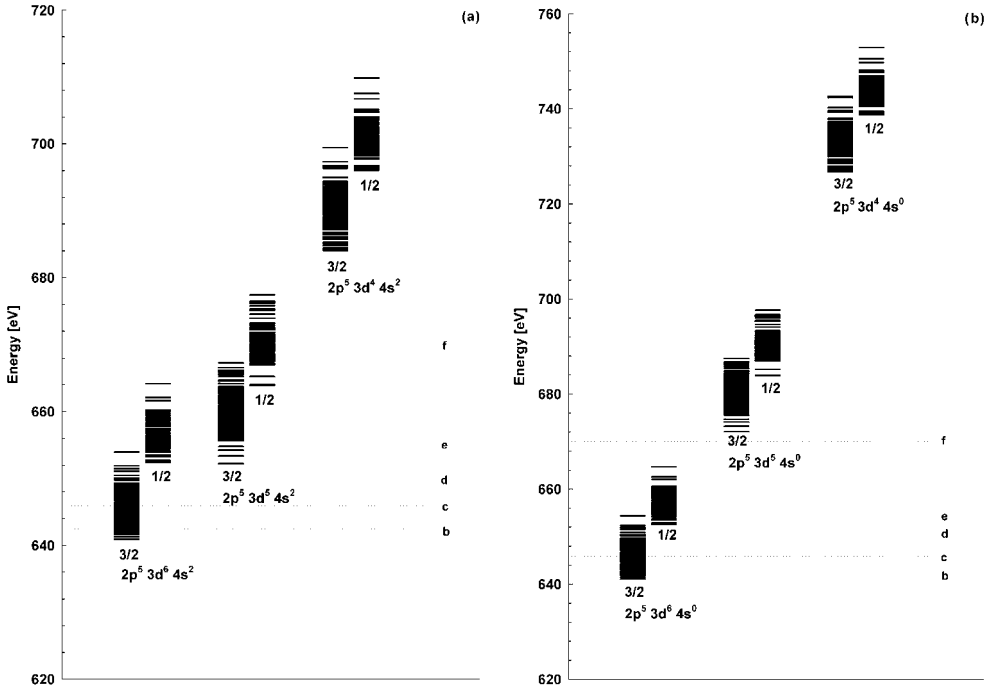

Figure 6. Energy level spectra of some configurations of atoms and ions of Mn. (a) Mn $2p^{-1}3d^64s^2$, Mn^+ $2p^{-1}3d^54s^2$ and Mn^{2+} $2p^{-1}3d^44s^2$; (b) Mn $2p^{-1}3d^6$, Mn^{2+} $2p^{-1}3d^5$ and $2p^{-1}3d^4$. The energies are indicated with respect to the ground level of Mn $2p^63d^54s^2$ or $2p^63d^5$. Excitation energies corresponding to various calculated emission spectra are indicated by a dotted line.

The general scheme of energy levels for the $2p^{-1}3d^N$ ($N = 4$–6) configurations with and without $4s^2$ electrons is shown in figure 6. Due to the strong interaction between the $2p^{-1}$ vacancy and the outer open $3d^N$ shell these energy spectra spread over a wide interval exceeding 20 eV. The spectra of $2p^{-1}_{1/2}3d^N$ and $2p^{-1}_{3/2}3d^N$ configurations are not separated energetically.

According to figure 6 the edges of photoionization for Mn and Mn^{2+} differ essentially by about 20 eV. This is in contrast to photoexcitation, where the shifts of the binding energies of 2p and 3d electrons due to the removal of $4s^2$ electrons almost compensate each other, while in photoionization it is caused by the shift of the binding energy of only the 2p electron. The L_3 (L_2) photoionization becomes possible for the atom at 652 (664) eV and for the ion at 672 (684) eV. The rapid change of the experimental XES spectrum with increasing excitation energy is related to the photoexcitation to various levels and finishes at about 660 eV; the slow change of the experimental spectra taken at larger energies must be related to the photoionization process. For this reason the model of the free Mn atom has been used for the interpretation of XES.

The experimental x-ray emission spectra were registered at various excitation energies related to the main structure of the photoabsorption spectrum. The comparison of the experimental and calculated absorption spectra enables us to determine the corresponding energies for the free Mn atom. Their positions are shown on the left side of the energy level spectrum.

Considering the photoexcitation as a resonant process, we have taken into account that the exciting x-ray beam has the spectral width equal to 0.53 eV and made the assumption

that the excitation of all levels finding themselves in such an interval is possible. During the photoionization all levels of an ion having energy lower than the energy of the exciting beam are more or less populated.

Various excitation and de-excitation processes influence the considered XES, thus the intensities of lines must be calculated using a general formalism [16]. The populations of the excited levels are determined from the condition that the number of atoms populating level i (ΔN_i^{in}) and depopulating it (ΔN_i^{out}) during a unit of time must be equal

$$\Delta N_i^{\text{in}} = \Delta N_i^{\text{out}}. \tag{1}$$

The number of atoms going into level i is expressed

$$\Delta N_i^{\text{in}} = \sum_s \sum_k N_k A^{(s)}(k \to i), \tag{2}$$

where N_k is the population of level k and $A^{(s)}(k \to i)$ is the rate of transition from level k to level i by process s. The summation in equation (2) is performed over all possible processes and levels. The initial levels of the considered XES at various energies can be populated by photoexcitation, photoionization and Auger transitions.

On the other hand, the number of atoms going out of level i is

$$\Delta N_i^{\text{out}} = N_i \sum_s \sum_k A^{(s)}(i \to k) = N_i A_i. \tag{3}$$

Here A_i is the total de-excitation rate of level i. In the atomic units it is equal to the natural width of the level. Due to the small fluorescence yields for the L_2 and L_3 vacancies only the Auger widths have been calculated in this work. Substituting equations (2) and (3) into (1) the general expression for the population of level i is obtained.

The intensities of emission lines have been calculated in the dipole approximation as the product of the population of the initial level, the radiative transition rate and the transition energy.

3.2.2. Dependence of x-ray emission spectra on photoexcitation energy. Depending on the value of excitation energy E_{exc} various processes—photoexcitation, photoionization and Auger transitions—can determine the population of levels from which the considered x-ray emission takes place. The calculated emission spectra for Mn are presented in figure 7.

According to figure 6(a) in cases b and c the energy of photons is sufficient only for the excitation L_3–$M_{4,5}$. The calculated b spectrum at the maximum of photoabsorption (figure 5(b)) reproduces reasonably two maxima of XES from figure 1. They both correspond to the transitions from closely lying levels of the same ^5D term of the $3d^6$ shell. The main maximum is determined by the transitions to the ground $3d^5\ ^6S_{2.5}$ level of the atom, i.e. to the transitions inverse to the photoexcitation; the other, low-energy maximum corresponds to the less probable transitions to various excited levels of the $3d^5 4s^2$ configuration.

In case c the excitation takes place practically to the single $2p_{3/2}^{-1}3d^6\ ^3D_2$ $J = 3/2$ level. The integral intensity diminishes with respect to the b spectrum—this corresponds to the less effective photoexcitation. The general features of the calculated and the experimental spectra are similar. The main maximum, in contrast to case b, corresponds to the transitions to the excited levels of the ground configuration (mainly to $3d^5\ ^4D_{3.5}$ and $3d^5\ ^4G_{4.5}$) and the considerably lower high-energy maximum to the single transition to the ground level.

E_{exc} for spectrum d corresponds to the energy interval where the upper levels of $2p_{3/2}^{-1}3d^6$ configuration overlap with the lower levels of $2p_{1/2}^{-1}3d^6$ configuration. In this region the photoexcitation is very weak. Small transition rates are usually calculated considerably less accurately than the rates of the strongest transitions.

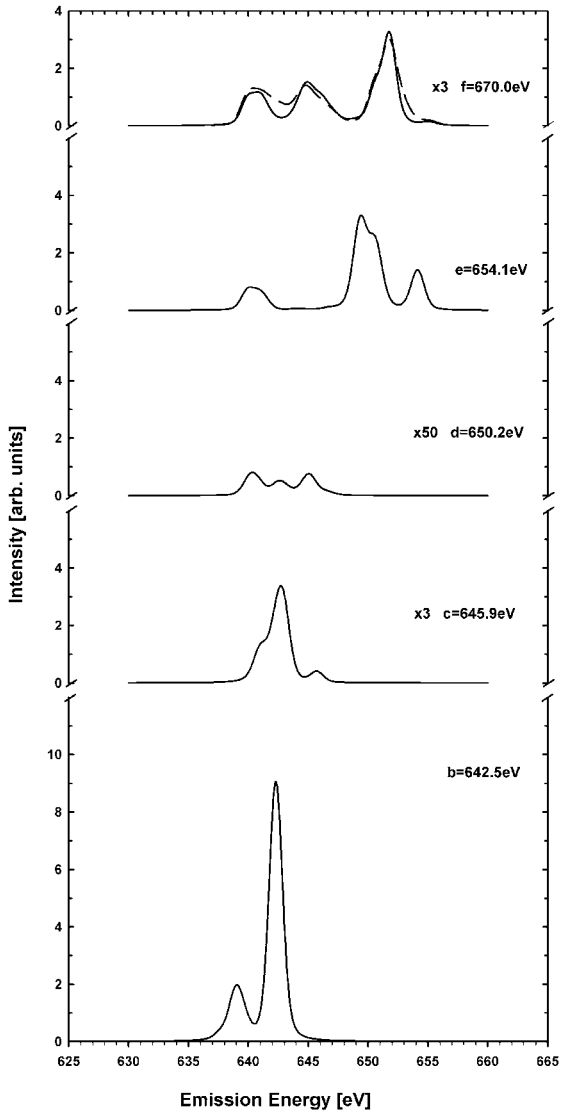

Figure 7. Variation of the calculated XES at various excitation energies of the Mn atom in the ground state $3d^5 4s^2$ (——). The excitation energies correspond to the indicated values in figure 6. The broken line in the f case corresponds to the calculation taking into account s–d mixing. In c, d and f cases the intensities of XES are multiplied by the indicated factors.

Spectrum e corresponds to the photo-absorption above the L_3 ionization limit. However, at $E_{\mathrm{exc}} = 654.1$ eV only the population of the lowest levels of configuration $2p_{3/2}^{-1}3d^5$ becomes possible by this process. On the other hand this value of E_{exc} corresponds to the maximal excitation to the levels of the $2p_{1/2}^{-1}3d^6$ configuration. In such a way two main maxima of spectrum e are generated. They appear as a result of the superposition of several lines. All the strongest lines originate from the mostly populated levels of the ^{5}D term of the d^6 shell and end in the ground level (smaller high-energy maximum) or in the other levels (higher low-energy maximum) of the $2p^6 3d^5$ configuration. During the photoionization the passive

$3d^5$ shell mainly remains in its $^6S_{2.5}$ ground state, and the most probable are the transitions to the many-electron states with the ^5D term of the $3d^4$ shell. In order to present the intensities of the radiative transitions in excited and ionized atoms on the same scale the photoionization was taken for the energy interval of continuum equal to the spectral width of the exciting beam. Transitions in the ions give a small maximum on the lower energy side. Such a maximum is seen in the experimental spectrum too.

The single ions can also be produced by the Coster–Kronig transitions shifting a vacancy from L_2 to L_3:

$$2p_{1/2}^{-1}3d^6 \rightarrow 2p_{3/2}^{-1}3d^4\varepsilon l. \tag{4}$$

However, the population of excited levels obtained by such a two-step process is essentially smaller than that by direct ionization and gives only about 10% contribution to the intensity of the same lines of XES in the interval 639–642 eV.

At the $E_{exc} = 668$ eV only the $L_{2,3}$ photoionization becomes possible. The energy spectrum of the $2p_{1/2}^{-1}3d^5$ configuration extends up to 680 eV; however, only the population of the lower levels, especially with the ^6S term of the $3d^5$ shell, is rather effective. Transitions from such levels with $2p_{1/2}^{-1}$ and $2p_{3/2}^{-1}$ vacancies give the two edge maxima of the f spectrum; the maximum in the middle corresponds to the group of transitions from other levels. The experimental spectrum has two maxima and a smaller structure between them. According to the calculations in the model used, the Coster–Kronig transitions (4) do not give a significant contribution to the f spectrum too. The calculated energies of XES maxima for the ions are shifted with respect to the experimental ones by about 4 eV. In order to obtain a better correspondence of the theoretical f spectrum to the experiment the calculations have been performed taking into account the s–d mixing; however, this does not lead to an essential change of the spectrum.

4. Conclusion

The comparison of the experimental and the theoretical Mn $L_{2,3}$ RXES of $Mn[N(CN)_2]_2$ shows that calculation in the atomic approach reproduces regularity in variation of the fine structure and energy position of RXES spectra. Indeed, the sharp intensity splashes are observed at L_3 and L_2 thresholds both in experiment and in theory. However, before the calculation the case of excitation at the L_2 threshold was unclear, because looking for the absorption spectra one can see that the excitation probability is much less for the L_2 level than for the L_3 level. Nevertheless, the calculations have shown that the integral intensities of RXES at L_3 and L_2 thresholds have close values. In between the thresholds RXES intensities are found to be dramatically reduced both in experiment and theory and the fine structure of spectra is reasonably reproduced by calculations. Some deviations in the calculated spectra are due to the fact that the emission in ionization channel appears in experiment beginning at excitation energy c, whereas in theory beginning at excitation energy d. Probably the parameters of intra-atomic interactions are decreased in solids because of the screening influence of interatomic electron density, which leads to the closeness of energy configurations corresponding to final states of ionization and excitation. It is not accidental that the energy positions of XAS and RXES maxima in atomic calculations are shifted to a high-energy range in comparison with experiment for ∼2 and ∼4 eV, respectively. This indicates the decrease of force parameters in solids.

We need to point out that the atomic calculation does not reproduce both fine structure and $I(L_2)/I(L_3)$ intensity ratio of ionization spectra above the L_2 threshold (f). Probably this is due to the impossibility of including the Coster–Kronig transitions in atomic calculations that are

forbidden in free ions and allowed in solids because of the energy closeness of configurations of the initial and the final states of radiationless transition.

Therefore, atomic calculation of Mn $L_{2,3}$ RXES reproduces dynamics of transformation of energy position, fine structure and relative intensities, revealing the many-electron origin of spectra. However, this approach cannot be used for description of ionization spectra. In this case a reasonable agreement in $I(L_2)/I(L_3)$ intensity ratio is achieved in the atomic calculation using C–K solid state parameters [12].

Acknowledgments

We would like to thank Alex Moewes for help in measurements and discussion of the obtained results. Funding by the Research Council of the President of the Russian Federation (grant NSH-1026.2003.2) and the Russian Science Foundation for Basic Research (project 05-02-16438) is acknowledged.

References

[1] Manriquez J M, Yee G T, McLean R S, Epstein A J and Miller J S 1991 *Science* **252** 1415
[2] Ferlay S, Mallah T, Quahes R, Veillet P and Verdauger M 1995 *Nature* **378** 701
[3] Manson J L, Kmety C R, Epstein A J and Miller J S 1999 *Inorg. Chem.* **38** 2552
[4] Kurmoo M and Kepert C J 1998 *New J. Chem.* **22** 1515
[5] Kmety C R, Manson J L, Huang Q, Lynn J W, Erwin R W, Miller J S and Epstein A J 1999 *Phys. Rev.* B **60** 60
[6] Kmety C R, Huang Q, Lynn J W, Erwin R W, Manson J L, McCall S, Crow J E, Stevenson K L, Miller J S and Epstein A J 2000 *Phys. Rev.* B **62** 5576
[7] Demchenko D O, Liu A Y, Kurmaev E Z, Finkelstein L D, Galakhov V R, Moewes A, Chiuzbaian S G, Neumann M, Kmety C R and Stevenson K L 2004 *Phys. Rev.* B **69** 205105
[8] Butorin S M 2000 *J. Electron Spectrosc. Relat. Phenom.* **110/111** 213
[9] Kotani A 2000 *J. Electron Spectrosc. Relat. Phenom.* **110/111** 197
[10] Butorin S M, Guo J-H, Magnuson M, Kuiper P and Nordgren J 1996 *Phys. Rev.* B **54** 4405
[11] Kurmaev E Z, Rehr J J, Ankudinov A L, Finkelstein L D, Karimov P F and Moewes A 2005 *J. Electron Spectrosc. Relat. Phenom.* **148/1** 1
[12] Krause M O 1979 *J. Phys. Chem. Ref. Data* **8** 307
[13] Karosene A V, Kiselev A A, Shadjuvene S D, Karazija R I, Zimkina T M and Fomichev V A 1974 *Izv. Akad. Nauk USSR Ser. Fiz.* **38** 426
[14] Gribov I V, Minin V I, Finkelstein L D and Nemnonov S A 1977 *Phys. Met. Metallogr.* **44** 643
[15] Cowan R D 1981 *The Theory of Atomic Structure and Spectra* (Berkeley, CA: University of California Press) p 731
[16] Karazija R 1996 *Introduction to the Theory of X-ray and Electronic Spectra of Free Atoms* (New York: Plenum)